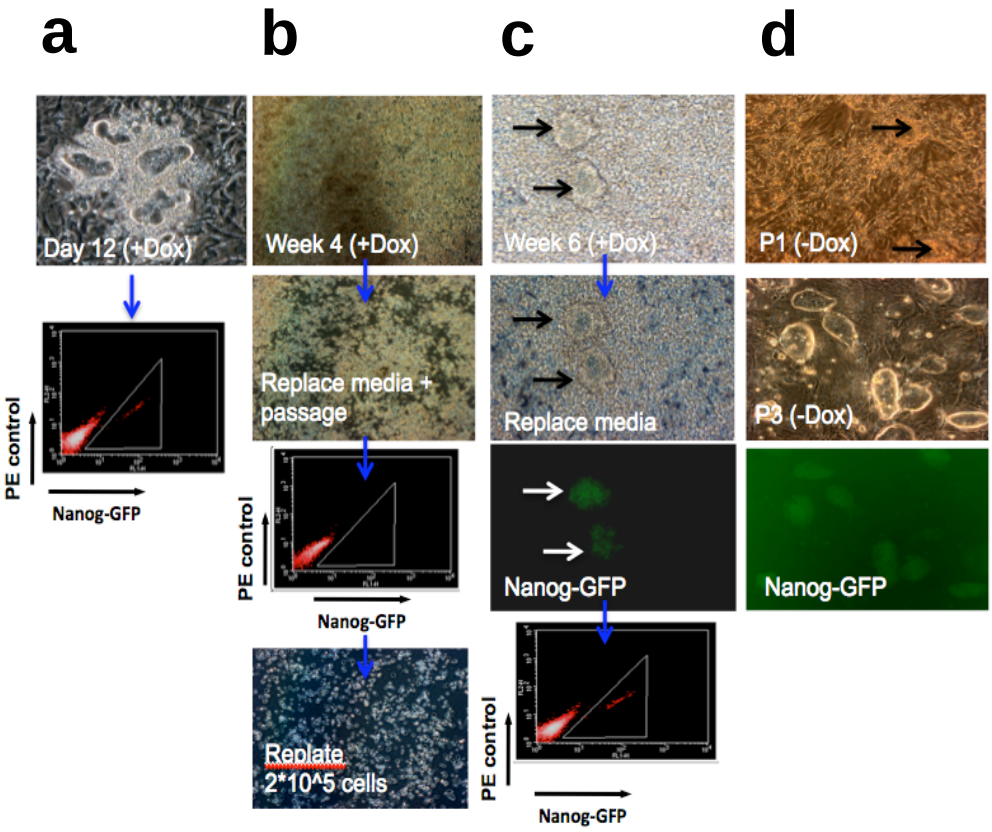

%Nanog-GFP+ *cells*

Sampled population	Non-adherent fraction	Non-adherent +adherent fraction
1	0	0
2	0	1.90
3	0	0.7
4	0	0
5	0	0.5
6	0	0
7	0	0
8	0	0
9	0	2.4
10	0	0
11	0	0
12	0	0
13	0	0
14	0	0
15	0	1.2
16	0	0
17	0	0
18	0	0
19	0	0
20	0	0
21	0	2.4
22	0	0
23	0	0
24	0	0
25	0	0
26	0	10.8
27	0	0
28	0	0
29	0	0
30	0	13.1
31	0	0
32	0	0
33	0	0
34	0	15.2
35	0	0

Supplementary Figure 1 | Strategy for long-term culturing and follow-up of monoclonal populations. Schematic with representative images and immuno-staining demonstrating the long term-culturing strategy. **a,** In the minority of cases, after single cell plating of Pre-B cells or monocytes in DOX, cells with ES-like morphology emerged (black arrow) and resulted in Nanog-GFP detection by FACS within 2 weeks. **b,** In the rest of the wells, non/semi adherent round cells grew that could be propagated in the presence of DOX. At the end of each week FACS was performed to test for the appearance of Nanog-GFP + cells, and when negative (as shown), approximately 2-2.5x10^5 cells were re-plated on gelatin and in the presence of DOX for continued follow-up analysis. **c,** This panel demonstrates the appearance of cells with ES-like morphology among the small round "intermediate cells". Nanog-GFP+ signal could be readily detected by microscope and FACS. **d,** Following detection of Nanog-GFP+ the cells were plated in the absence of DOX, and iPSC colonies were readily observed (black arrows) while partially reprogrammed non-adherent cells ceased to grow by DOX withdrawal. Stable iPSC Nanog-GFP lines were established and expanded by 1-2 passages. **e,** Results of FACS analysis for GFP detection performed on randomly selected monoclonal populations from different experimental groups. Middle column shows results on non-adherent fraction of cells only obtained from the supernatant of growing wells. The analysis shows that Nanog-GFP iPS cells can be detected only in the samples the contain the adherent fraction, consistent with iPSCs being fully adherent on gelatin coated tissue culture dishes. % of Nanog-GFP+ cells is indicated.

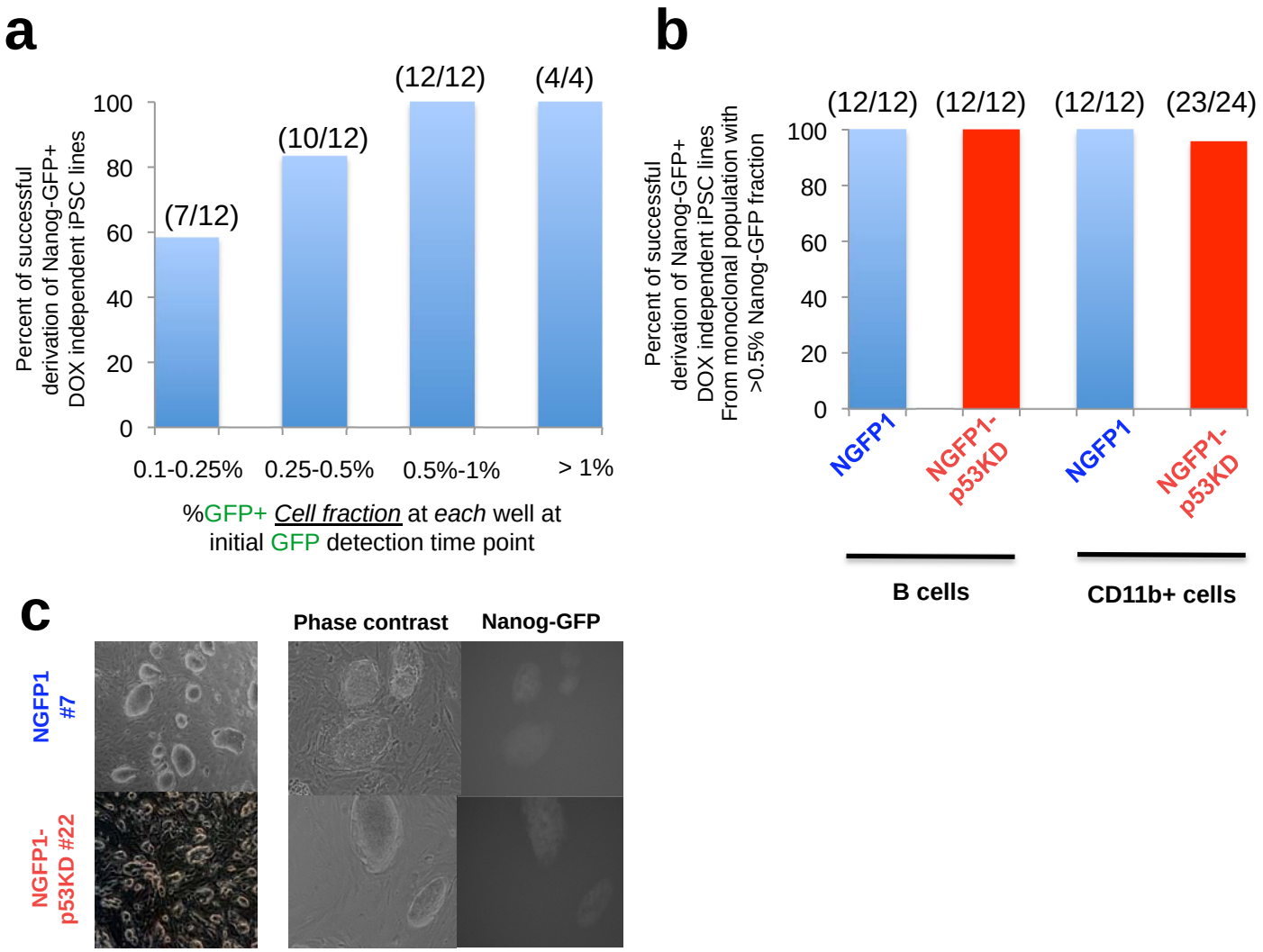

Supplementary Figure 2 | Threshold for isolation of DOX-independent Nanog-GFP+ iPSC lines. a, Experiments to determine the FACS detection threshold for Nanog-GFP in order to classify a given well as "being reprogrammed". As described in Fig. 2a, B cells were isolated from NGFP1 chimeras. Next, single cells were cloned and grown in the presence of DOX. After five weeks of DOX induction, clonal populations were analyzed for the percentage of Nanog-GFP+ cells in each population and sub-grouped into four categories based on Nanog-GFP fraction: 0.1%-0.25%, 0.25%-0.5%, 0.5%-1%, and >1%. Cells were subsequently grown in the absence of DOX and were passaged at least twice. Each cell population was scored for the presence of DOX-independent Nanog-GFP+ clones. The presence of 0.5% GFP+ cells in a given well reproducibly facilitated the isolation of DOX-independent Nanog-GFP+ iPSC lines. **b,** Experiments described in (**a**) were performed with various different cell types: wild-type and p53KD B cells and CD11b+ myeloid cells. Data only from wells in which initial detection of Nanog-GFP+ was >0.5% are shown. This analysis demonstrates that a Nanog-GFP+ detection threshold of 0.5% is a reliable marker for isolation of iPSCs across different donor cell types. **c,** Representative images of iPSC lines isolated and detection of endogenous Nanog-GFP.

a

	B cell (- DOX)	B cell (3d on DOX)	B cell (5d on DOX)
CD43	>95%	36%	3%
CD19	>95%	41%	2%
CD45	>95%	31%	0%
IL-7R	>95%	29%	2%
SSEA1	0%	0%	8%

b

	#66,w5;- (GFP+ on w13)	#1,w5;- (GFP+ on w12)	#1,w8;- (GFP+ on w12)	#53,w3;- (GFP+ on w5)	#59,w10;-	#20,w8;- (GFP+ on w10)	#4,w13;-
CD43	0%	0%	0%	0%	0%	0%	0%
CD19	0%	0%	0%	0%	0%	0%	0%
CD45	0%	0%	0%	0%	0%	0%	0%
IL-7R	0%	0%	0%	0%	0%	0%	0%
SSEA1	25%	19%	0%	0%	15%	0%	8%

Supplementary Figure 3 | Characterization of B cell populations following DOX induction. a, Isolated B cells were cultured in the presence of DOX and tested for surface expression of the indicated markers at time 0 (-DOX) and 3 and 5 days on DOX. Consistent with previous reports (Mikkelsen et al. *Nature* 2008 and Stadtfeld et al. *Cell Stem Cell* 2008) somatic cell markers (CD43, CD19, CD45 and IL-7R) were efficiently silenced by 5 days of transgene induction. Percentage of positive cells is indicated in comparison to isotype match antibody control. **b,** FACS analysis of surface markers after OSKM transgene induction in reprogramming Pro B derived samples grown in the presence of DOX. Percent of positive cells is indicated in comparison to isotype match antibody control. Information regarding each clone is presented as: clone #, week on DOX induction was tested, Nanog-GFP+ >0.5% status, and week # when Nanog-GFP+ became significantly detected (>0.5%). Note that all reprogramming populations had lost expression of B/hematopoietic cell markers consistent with suppression of somatic cell identity (shown in a). SSEA1 detection was heterogeneous between different populations and was not a predictive parameter for whether a monoclonal populations would give rise to iPSC at relatively early or late time points (compare clone #66 and #53). These results are consistent with fluctuating expression pattern of SSEA1 surface marker during reprogramming (note clone #1 at w5 and w8 and Mikkelsen et al. *Nature* 2008).

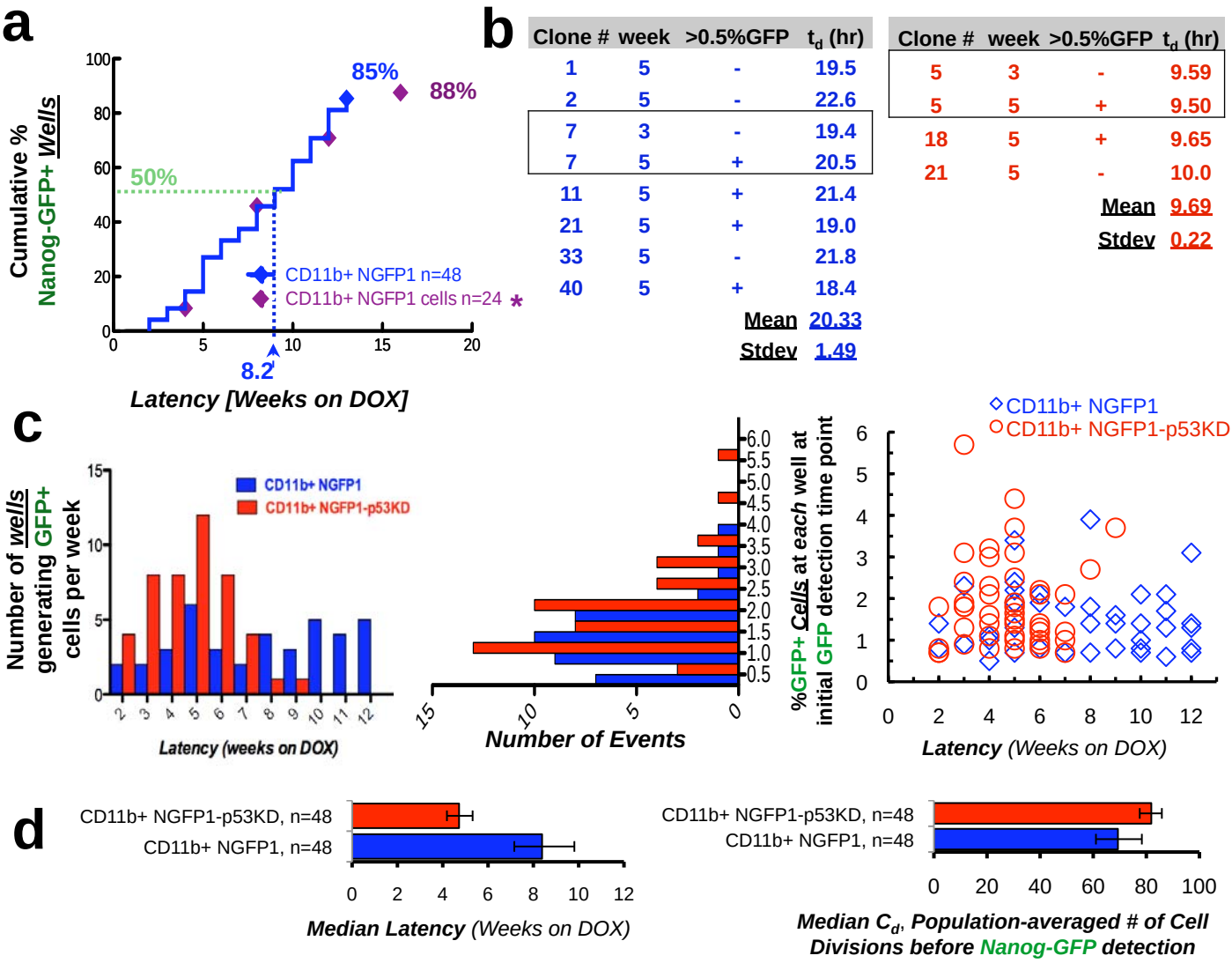

Supplementary Figure 4 | Reprogramming of CD11b+ derived cell populations. a, CD11b+ derived cells were seeded as single cells and cultured in DOX. Reprogramming of NGFP1 clonal CD11b+ populations was measured as the cumulative number of wells that became Nanog-GFP+ over time. After 13 weeks, greater than 85% of wells generated iPSCs, and after 16 weeks greater than 88% of wells generated iPSCs. Asterisk indicates that measurements were taken every 4 weeks. **b,** Exponential growth described the growth well for each clone (R^2=0.97-1.0), and doubling time, t_d, was calculated from these fits. No difference in doubling times was statistically significant (p<0.05) except between NGFP1 (blue) versus NGFP1-p53KD (red) groups. **c,** Left: For reprogramming of CD11b+ wells, the number of wells generating Nanog-GFP+ cells each week is plotted against the time in DOX containing medium. Right panel shows the %Nanog-GFP+ cells for each individual well (open markers) at the week when GFP was initially detected (>0.5% GFP+). Horizontal solid lines represent the average value of GFP+ fraction in the populations upon initial detection of a positive signal (defined >0.5% in the study; see Supplementary Fig. 2) and indicate no significant difference between NGFP1 and NGFP1-p53KD populations (1.54% and 1.85%, respectively [p>0.05]). **d,** Median times and cell divisions during latency determined through parametric statistical analysis as described in Supplementary Fig. 12. Notably, transgene induction levels where highly similar between monocytes and B cell populations (Supplementary Fig. 8), possibly explaining the similar reprogramming kinetics observed for the two distinct cell types.

a

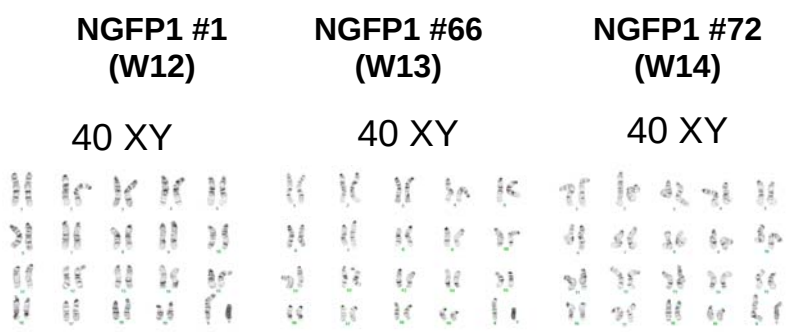

b

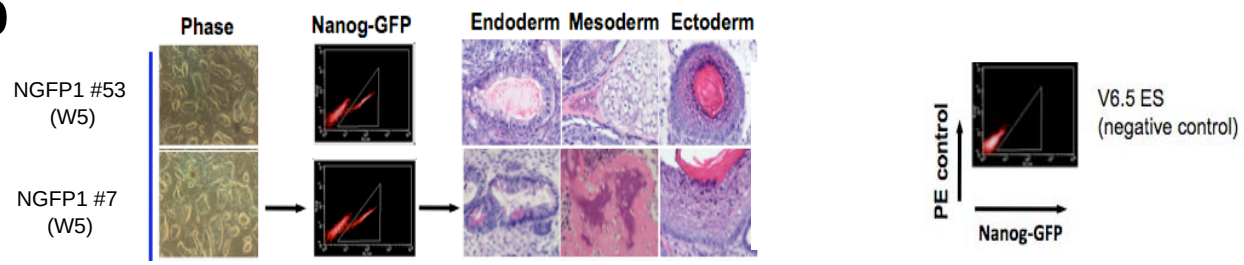

c

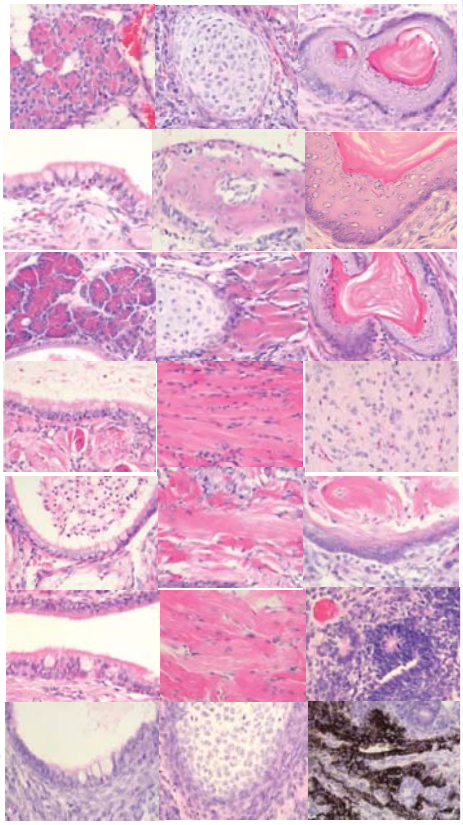

	Nanog-GFP	Oct4	Sox2	SSEA-1	AP
NGFP1 #1 (W12)	+	+	+	+	+
NGFP1 #66 (W13)	+	+	+	+	+
NGFP1 #72 (W14)	+	+	+	+	+
NGFP1 #47 (W10)	+	+	+	+	+
NGFP1 #20 (W10)	+	+	+	+	+
NGFP1 #9 (W3)	+	+	+	+	+
NGFP1 #16 (W5)	+	+	+	+	+

Supplementary Figure 5 | See figure legend on next page.

d NGFP1 #72 (W14)

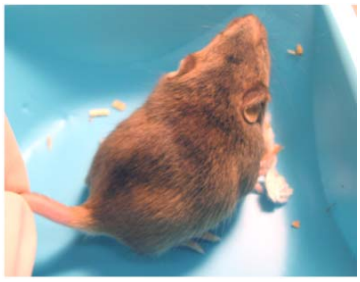

Supplementary Figure 5 | Characterization of NGFP1 Pre-B derived iPSC clones at different times following DOX induction. **a-c**, Randomly selected iPSC lines were selected for analysis. Clone # is indicated for each panel and time on DOX required to derive each line is indicated in parenthesis (W; weeks on DOX). **a,** Normal karyotype was observed by analyzing different iPSC clones derived after 12-14 weeks on DOX. **b,** Characterization of B cell derived and DOX-independent iPSCs demonstrating ES-like morphology, specific Nanog-GFP reporter detection by flow cytometry, and ability to generate *in vivo* differentiated teratomas. **c,** Well differentiated teratomas were derived from all lines tested with evident formation of endoderm, mesoderm and ectoderm structures. Table on the right summarizes the results of immunostaining / fluorescent detection of the indicated markers on the DOX-independent iPSC clones. **d,** Chimera generated following injecting NGFP1 #72 iPSC clone derived after 14 weeks on DOX induction *in vitro*. High contribution is evident by the agouti coat color.

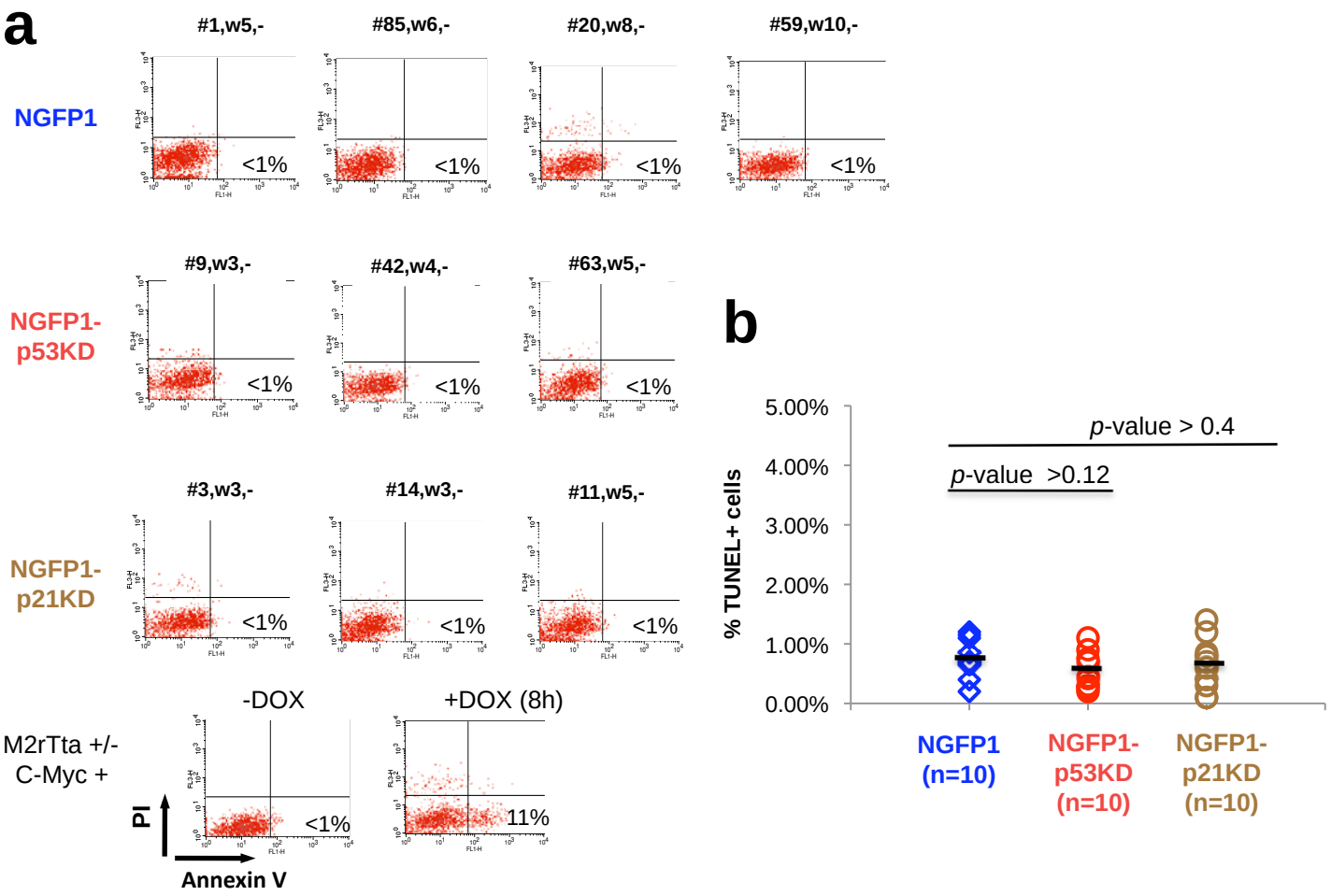

Supplementary Figure 6 | Background apoptosis levels in reprogramming populations from NGFP1 B cells. Apoptosis rates were quantified in reprogramming populations obtained from NGFP1, NGFP1-p53KD and NGFP1-p21 KD B cells. **a,** Annexin V- FITC and propidium iodide staining on randomly selected clones are shown, and demonstrate background (<1%) levels of apoptotic fraction (AnnexinV+ PI- in lower right quadrants). Information regarding each clone is presented as: clone #, week on DOX when then induction test was performed, Nanog-GFP+ >0.5% status. We verified a Nanog-GFP negative signal before analysis to avoid false positive detection of Annexin V FITC. Pro/Pre B cells were isolated from a mouse carrying only the c-Myc transgene and Rosa26-M2rTta and grown for 3 days on OP9 feeders in the presence of IL-7 (Markoulaki et. al. *Nature Biotechnology* 2009). Early apoptosis was quantified following 8 hr of DOX mediated c-Myc transgene induction. **b,** Flow cytometry based terminal deoxynucleotidyl transferase dUTP nick and labeling (TUNEL) assay was also performed on randomly selected cells throughout the process (weeks 3-10 on DOX). This independent analysis confirmed insignificant levels of apoptotic cells in the DOX supported populations. These results are consistent with the notion that Oct4, Sox2, c-Myc and Klf4 could act in concert as context dependent oncogenic and anti-apoptotic factors enabling hematopoietic cell propagation in the context of optimized OSKM transgenes expression without additional transformation.

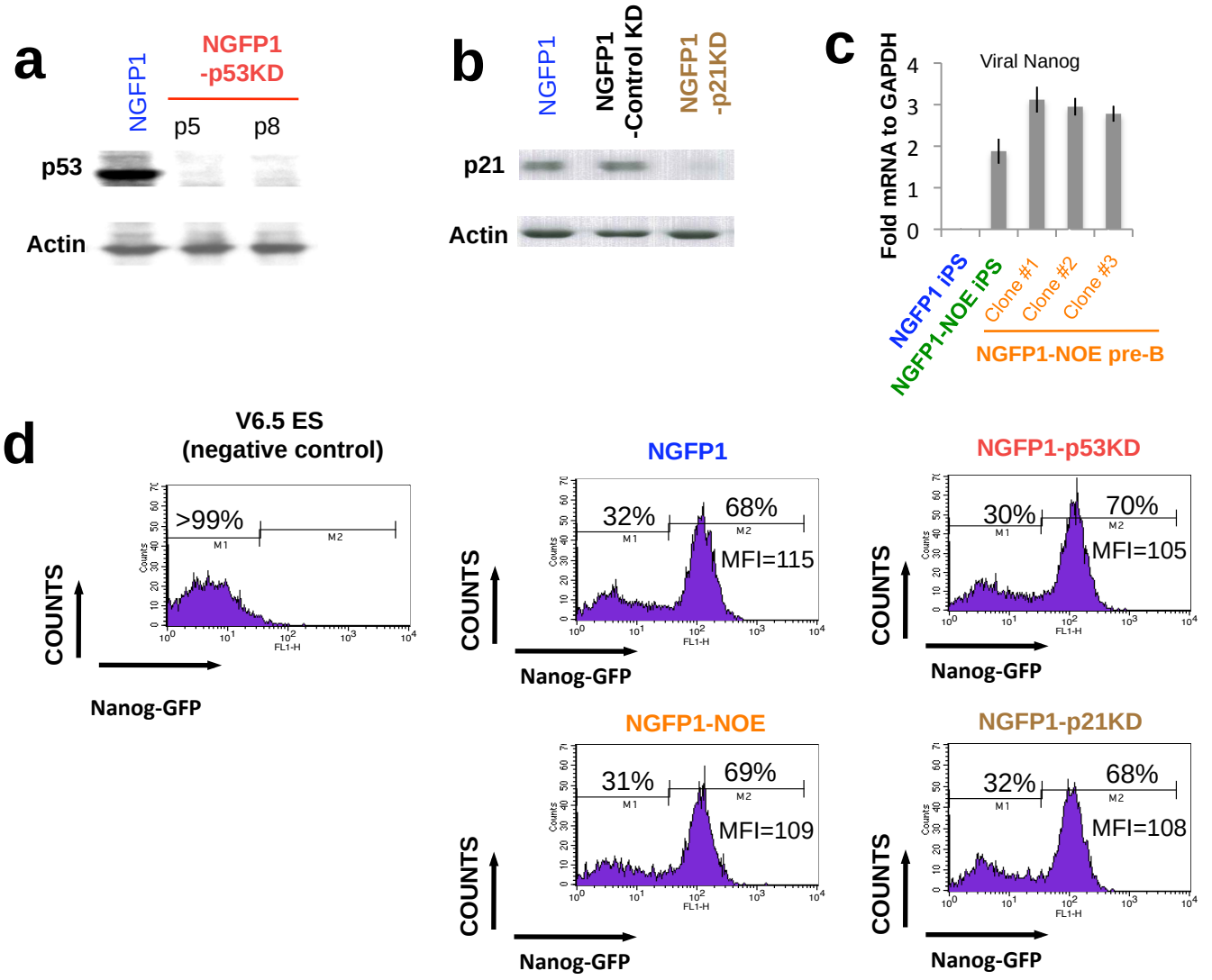

Supplementary Figure 7 | Characterization of NGFP1 primary iPSC lines used. **a-b,** NGFP1 iPSCs were infected with lentivirus PsicoR plasmid encoding hairpins against mouse *p53*, *p21* and *CD8* (used as control against an irrelevant gene). Infected cells were subcloned and viral integration was verified by PCR specific detection. Knockdown was specifically verified by western blotting on the selected subcloned lines (NGFP1-p53KD, NGFP1-p21KD and NGFP1-Ctrl KD). **c,** NGFP1 line was infected with a TetO-Nanog virus, and viral transgene integration was verified by southern and PCR (data not shown). Nanog expression was verified by RT-PCR in NGFP1-NOE (Nanog over-expresser) iPSC line and derived B cell clones (1-3) grown in the presence of DOX. **d,** FACS analysis for NGFP1 iPSC lines with and without additional genetic perturbations. Cells were pre-plated on gelatin before the analysis to deplete feeders and differentiated fractions. The previously described biphasic pattern of Nanog expression (Chambers et al. *Nature* 2007) was not altered by modulating the p53 pathway or overexpressing Nanog. Moreover, the median fluorescence intensity (MFI) of Nanog-GFP+ positive cells was not significantly altered.

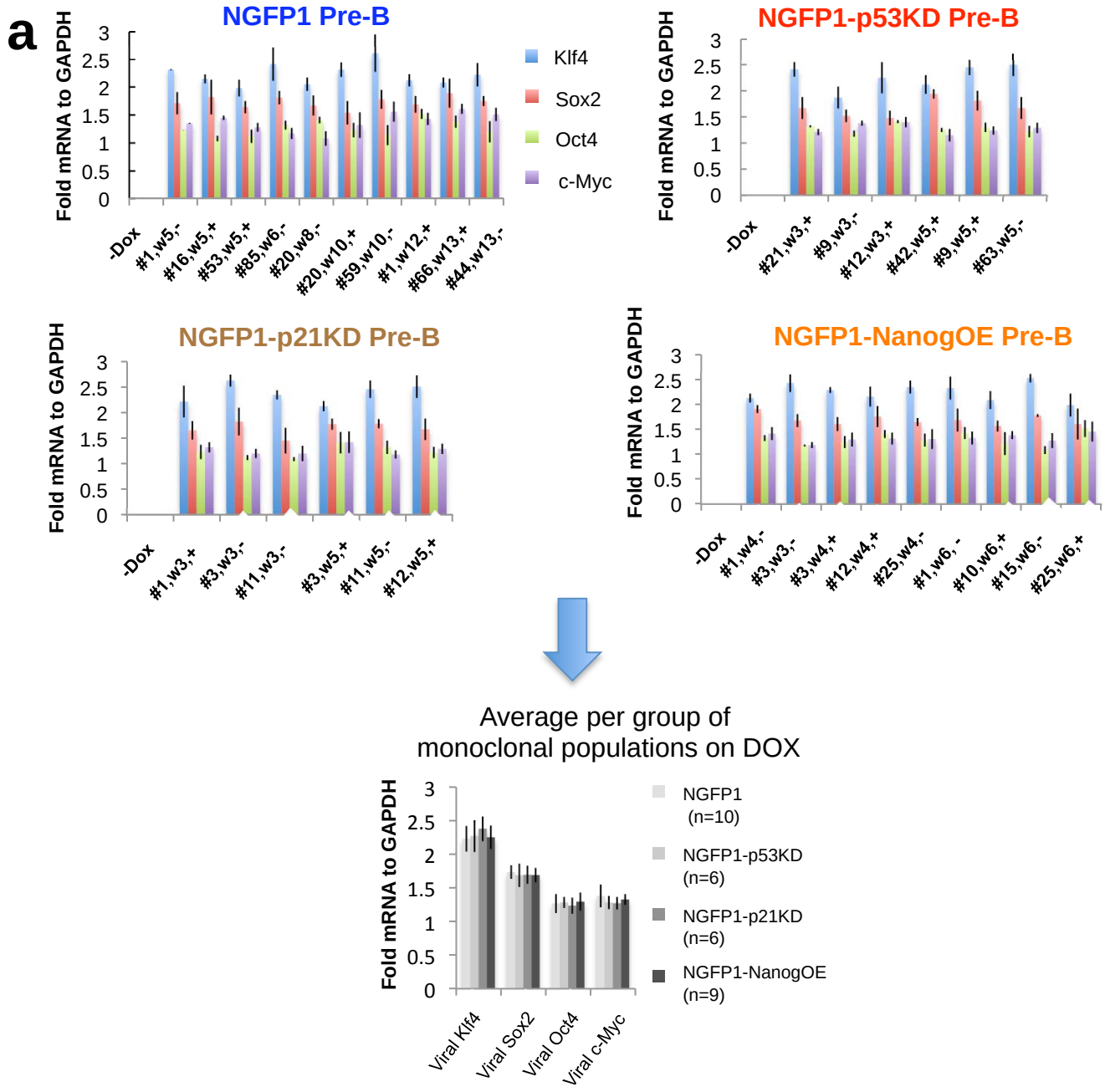

Supplementary Figure 8 | See figure legend on next page.

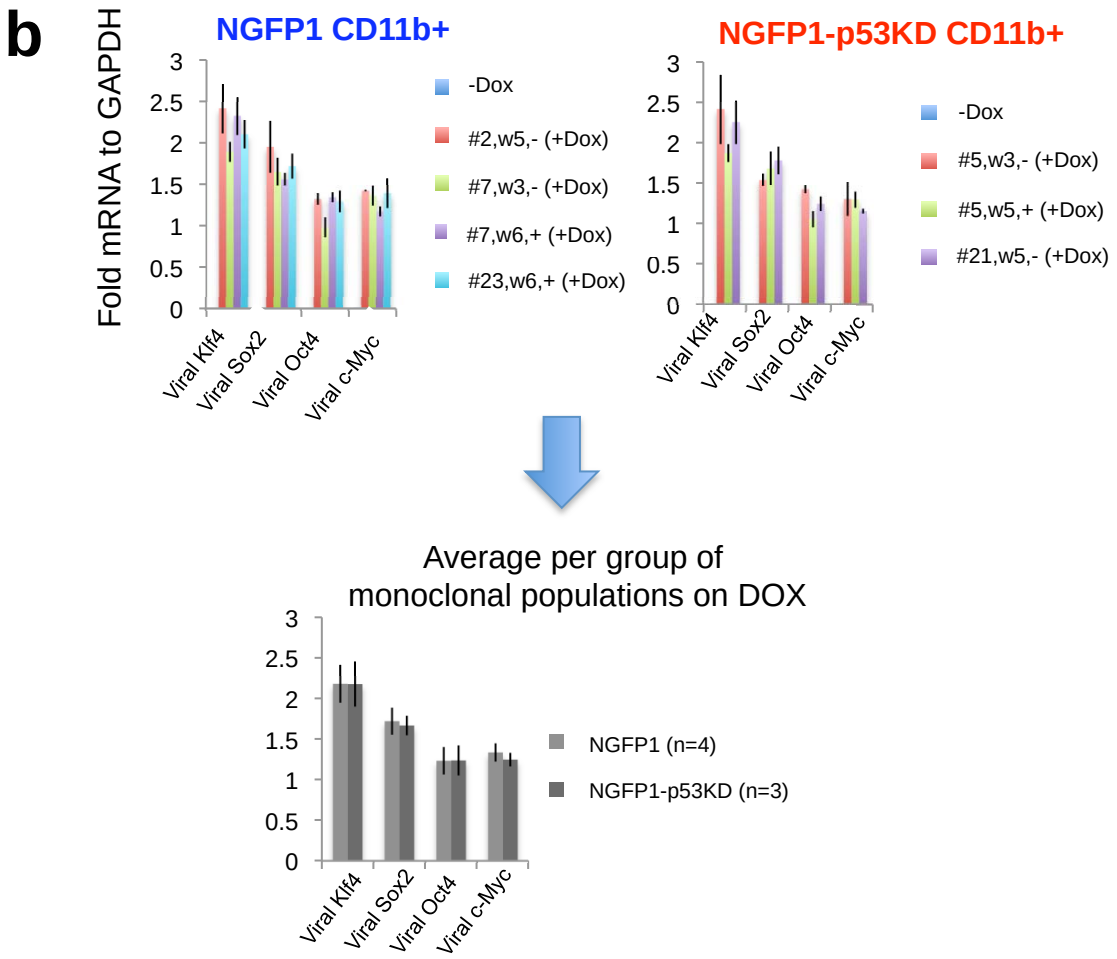

Supplementary Figure 8 | Summary for transgene induction levels. RT-PCR analysis of OSKM transgene induction levels in reprogramming B (**a**) and CD11b+ (**b**) derived samples grown in the presence of DOX. Average relative expression levels and standard deviation from 2-3 RT-PCR reactions are shown for all four factors. Polyclonal freshly isolated cells grown in the absence of DOX were used as negative controls. Information regarding each clone is presented as: clone #, week on DOX induction was tested, Nanog-GFP+ >0.5% status. Average induction levels for OSKM in different genetic backgrounds following genetic perturbation are also summarized in the lower part of each subpanel. Overall the results indicate that transgene expression was not altered by the different perturbation and that difference in transgene expression was not an underlying cause for the difference in reprogramming latencies between monoclonal population within each experimental group.

NGFP1-p53KD

Clone #	week	>0.5%GFP	t_d (hr)
1	3	+	9.50
2	3	-	9.17
2	5	-	9.48
4	3	+	9.80
9	3	-	9.62
9	5	+	9.40
22	3	-	9.37
42	5	+	9.77
17	3	-	9.70
17-iPS	N/A	+	10.2
p53KD-iPS	N/A	+	10.2

NGFP1-Lin28OE

Clone #	week	>0.5%GFP	t_d (hr)
1	3	-	13.2
1	4	-	12.9
1	7	+	13.8
2	3	-	13.2
2	4	+	13.2
8	3	+	13.2
44	4	-	13.4
44	7	-	13.4
50	7	-	13.7
Lin28OE-iPS	N/A	+	13.6

NGFP1-p21KD

Clone #	week	>0.5%GFP	t_d (hr)
1	3	+	9.66
3	3	-	9.88
3	5	+	9.86
10	3	+	9.54
11	3	-	9.92
11	5	-	10.0
12	3	-	9.76
12	5	+	9.59
22	5	-	9.78
25	5	+	9.86
30	5	-	9.90
p21KD iPS	N/A	+	10.0

NGFP1-NanogOE

Clone #	week	>0.5%GFP	t_d (hr)
1	4	-	17.0
1	7	+	16.3
10	4	-	16.5
10	6	+	16.7
15	4	-	16.5
15	7	-	17.0
25	4	-	17.2
25	6	+	16.1
32	6	-	16.4
32	7	+	15.9
41	6	-	16.8
41	7	+	16.7
NOE-iPS	N/A	+	14.8

Supplementary Figure 9 | Proliferation data for perturbed NGFP1 monoclonal populations. Tables show the doubling time (t_d) for each Pre-B derived clonal population, listed as "clone #, weeks on DOX, Nanog-GFP >0.5% status (+ or -)." Boxed rows delineate cases where the same clonal population was measured at different times during DOX induction or after iPSC isolation. Lower lines labeled in green indicate data obtained on subcloned or parental iPSC lines. No difference in doubling times was statistically significant (p<0.05) except between the different perturbation groups.

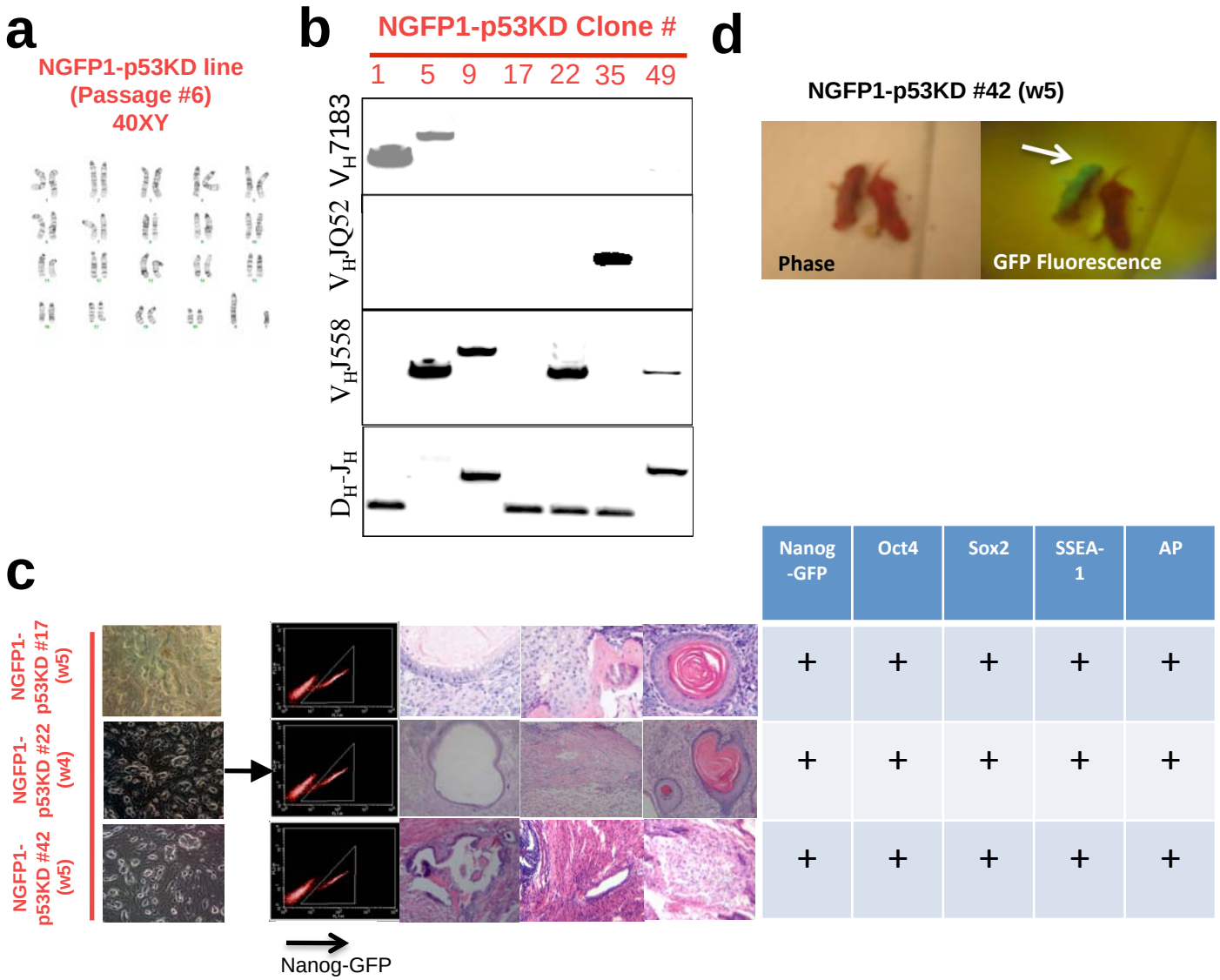

Supplementary Figure 10 | Characterization of NGFP1-p53KD B cell derived iPSC clones. a, NGFP1-p53KD primary iPSC line showed normal karyotype at early passage (P6) and was injected into blastocysts to generate chimeras from which Pre-B were derived for long term analysis. **b,** The NGFP1-p53KD B cell donor cells were derived from 3-5 week old mice; all analyzed clones carried different heavy chain rearrangement patterns, arguing against the possibility that cells in individual wells were derived from a B cell tumor which may have resulted following p53 knockdown (which would be expected to be mono/oligo clonal). **c,** Well differentiated teratomas were derived from all lines tested with evident formation of endoderm, mesoderm and ectoderm structures. Table on the right summarizes the results of immunostaining / fluorescent detection of the indicated markers on the DOX independent iPSC clones derived. Clone # is indicated for each panel and time on DOX required to derive each line is indicated in parenthesis (w; weeks on DOX). **d,** Chimera generated following injecting NGFP1-p53KD #42 iPSC clones derived following 5 weeks on DOX induction *in vitro*. Prior to injection the cell line was labeled with a constitutively expressed lentiviral GFP expressing vector, and chimerism is evident by specific GFP detection by fluorescent lamp (highlighted by the white arrow).

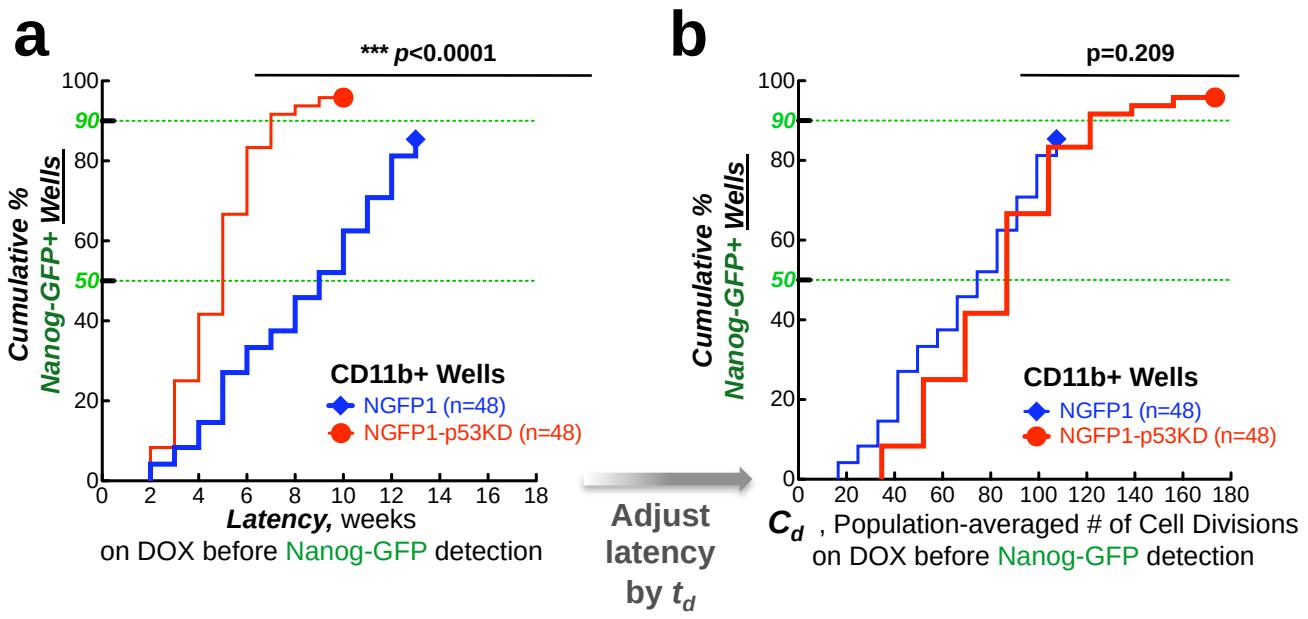

Supplementary Figure 11 | Reprogramming of NGFP1-p53KD CD11b+ derived cell populations.
As in Fig. 3c-d, latencies for reprogramming various clonal CD11b+ donor cell derived populations.

a

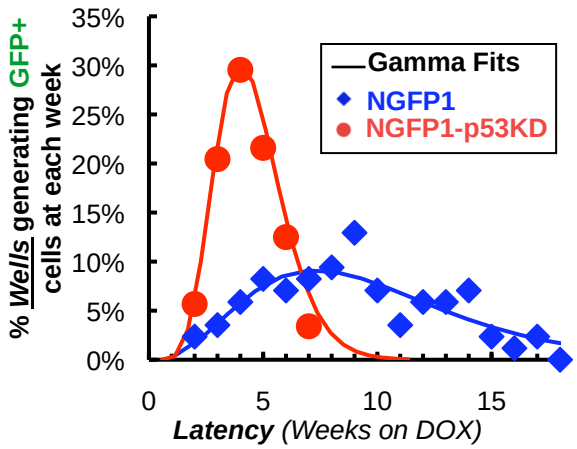

Parametric Distribution	Location parameter	Shape parameter	Scale parameter	χ^2
Gamma	N/A	5.1±0.3	16±1	107
Weibull	N/A	2.7±0.1	89±2	113
Lognormal	4.3±0	N/A	0.49±0.02	114
Normal	78±1	N/A	30±1	133
Extreme Value	95±2	N/A	30±1	242

b

Well Type	Compared to NGFP1 B cell parametric gamma function fit	Compared to NGFP1 B cells using non-parametric log-rank test					
	C_d data	Time data			C_d data		
	χ^2	χ^2	*p*-value	Increase	χ^2	*p*-value	Increase
NGFP1 CD11b+ cells	1.1	0.38	0.5401	N	1.2	0.272	N
NGFP1-p53KD B cells	89	145	< 0.0001	Y	0.42	0.518	N
NGFP1-p21KD B cells	90	124	< 0.0001	Y	0.011	0.915	N
NGFP1-Lin28OE B cells	52	35	< 0.0001	Y	0.96	0.327	N
NGFP1-NanogOE B cells	300	96	< 0.0001	Y	41	< 0.0001	Y

c

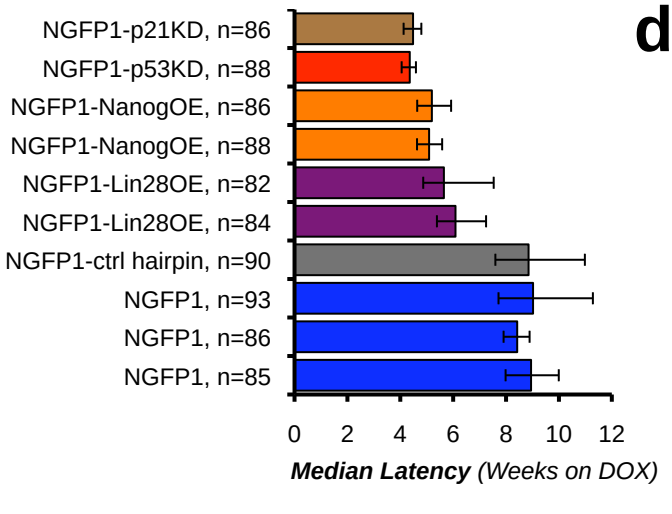

d

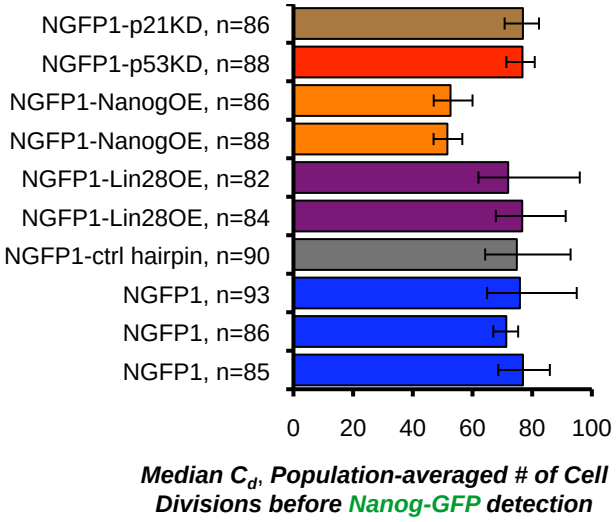

Supplementary Figure 12 | Median latencies with parametric and non-parametric numerical analyses. **a,** For each week, the percent of wells generating iPSCs is plotted for B cell NGFP1 and NGFP1-p53KD wells. The solid line is the fitted gamma distribution for the two types of wells. Table on right lists the fit of various two-parameter distributions and the associated chi-squared goodness of fit statistic (χ^2) for all the events seen in the cell-division rate dependent acceleration and NGFP1 B cell cases. Lower χ^2 indicate better fits. **b,** Statistics for comparing different reprogramming dynamics against both time and cell divisions (C_d) between the well type listed on the left and NGFP1 B cell wells. The "Increase" column signifies a *p*-value<0.05 and that the cumulative probability of wells generating iPSCs increased over the NGFP1 B cell case. **c,** Median latency times and 95% confidence intervals were calculated from best parametric gamma fits. For *p*-values see part b. **d**, Parametric analysis on latency data with cell division number yielded the median number of cell divisions during latency and 95% confidence intervals. For *p*-values see part b.

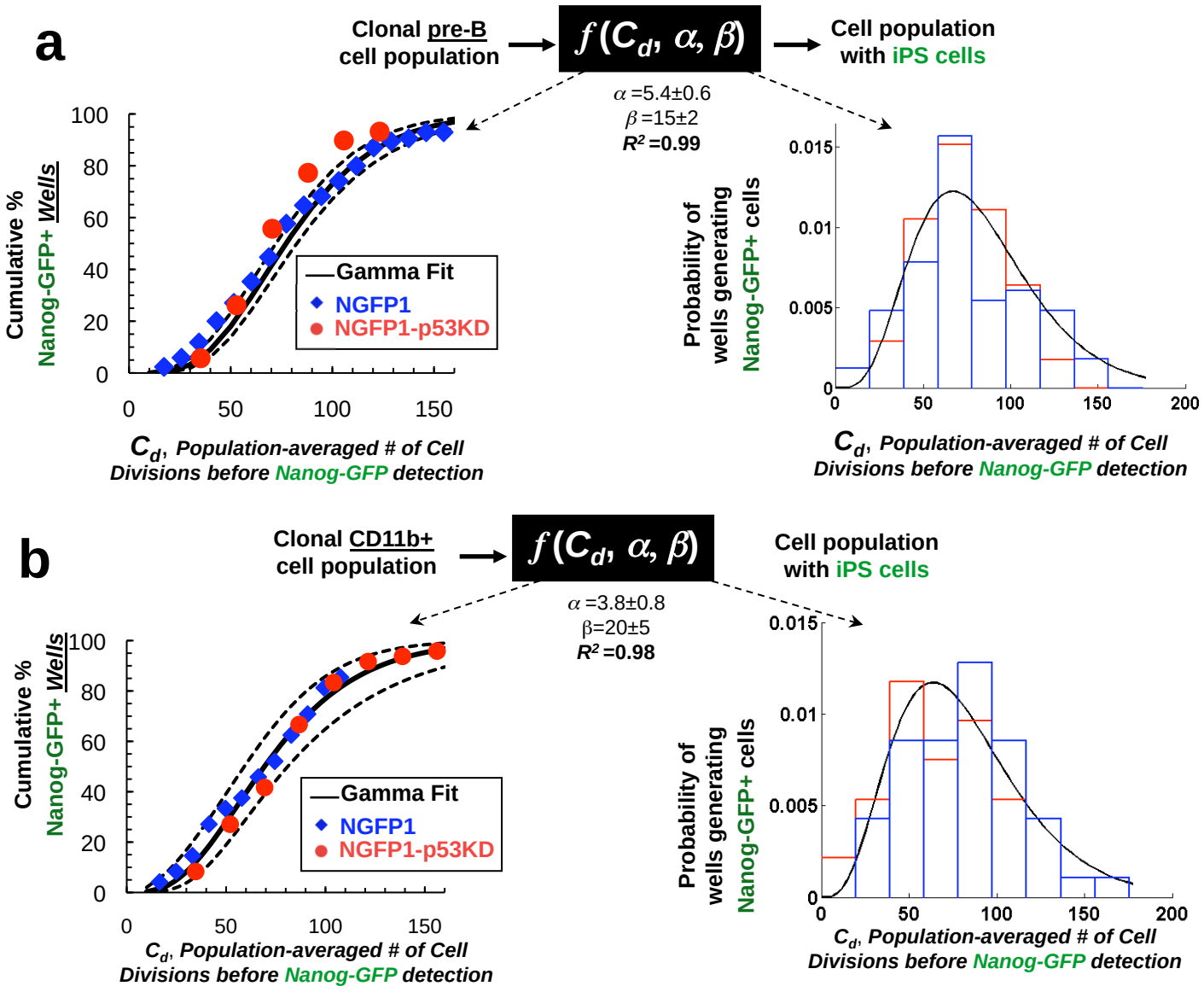

Supplementary Figure 13 | Parametric analysis of reprogramming events observed in NGFP1 and NGFP1-p53KD monoclonal populations. a, Using data from Fig. 3c-d, a gamma distribution was used to fit the events observed (see parametric analysis summary in Supplementary Fig. 12; dashed lines indicate 95% confidence interval). The cumulative number of wells that became Nanog-GFP+ for both NGFP1 and NGFP1-p53KD B cell derived lines were similar when time is rescaled by doubling time. The probability density of generating Nanog-GFP+ cells (derivative of the left) is shown in the right panel. This fit gamma distribution describes the probability of rate-limiting events occurring as a function of cell division (right) as the monoclonal population grows from a single cell. These events do not necessarily reflect changes at the single cell level and rather describes changes in the bulk population. **b,** Identical analysis as described in part a for NGFP1 and NGFP1-p53KD CD11b+ cell derived lines (using data in Supplementary Fig. 11).

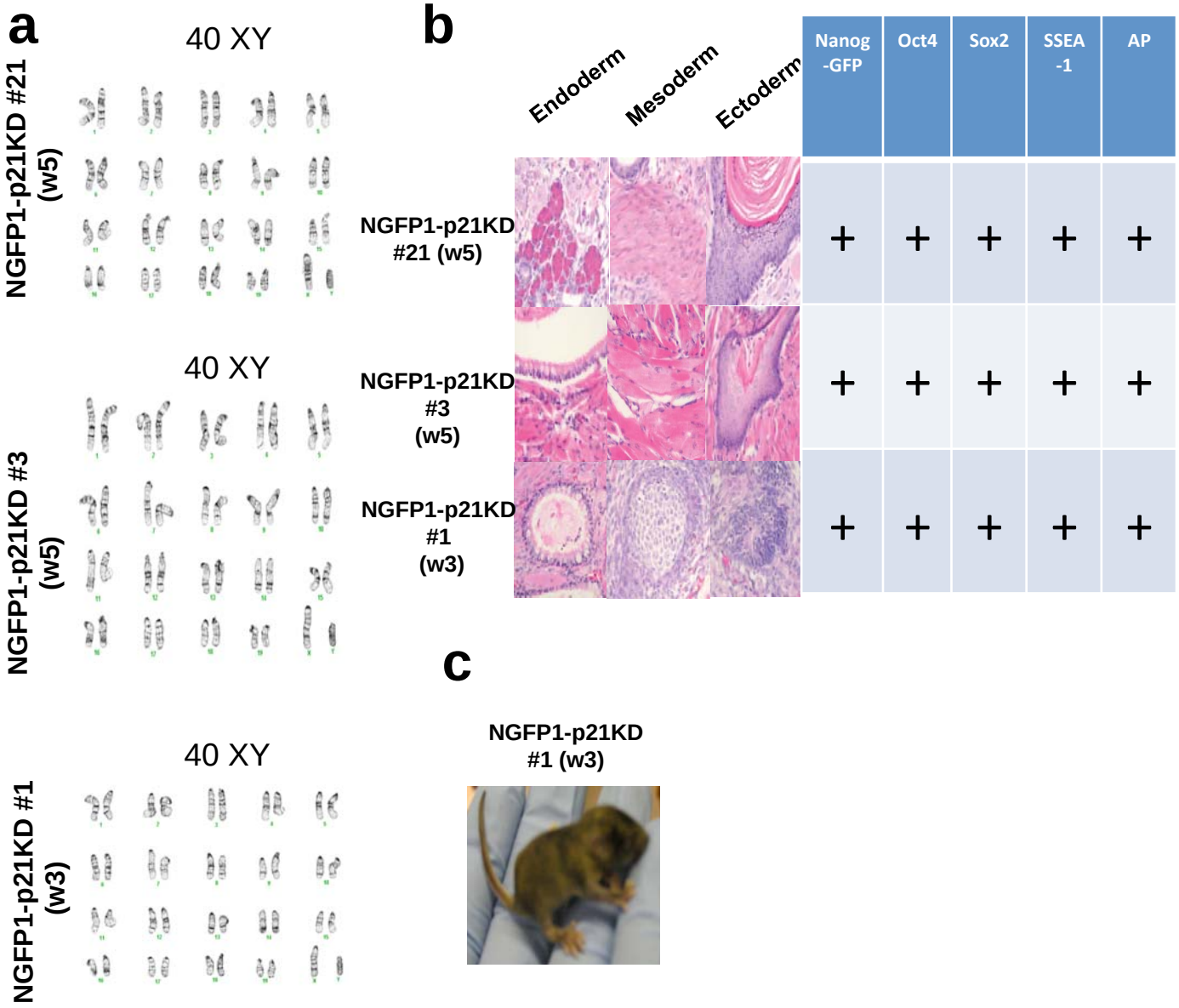

Supplementary Figure 14 | Characterization of NGFP1-p21KD B derived iPSC clones. a, Randomly selected NGFP1-p21KD B cell derived secondary iPSC lines showed normal karyotype when tested at passage 5. Clone # is indicated for each panel and time on DOX required to derive each line is indicated in parenthesis (w; weeks on DOX). **b,** Well differentiated teratomas were derived from all lines tested with evident formation of endoderm, mesoderm and ectoderm structures. Table on the right summarizes the results of immuno-staining / fluorescent detection of the indicated markers on the DOX independent iPSC clones derived. Clone # is indicated for each panel and time on DOX required to derive each line is indicated in parenthesis (w; weeks on DOX). **c,** Chimera generated following injecting NGFP1-p21KD #1 iPSC clone derived following 3 weeks on DOX induction *in vitro*. Chimerism is evident by the agouti coat color.

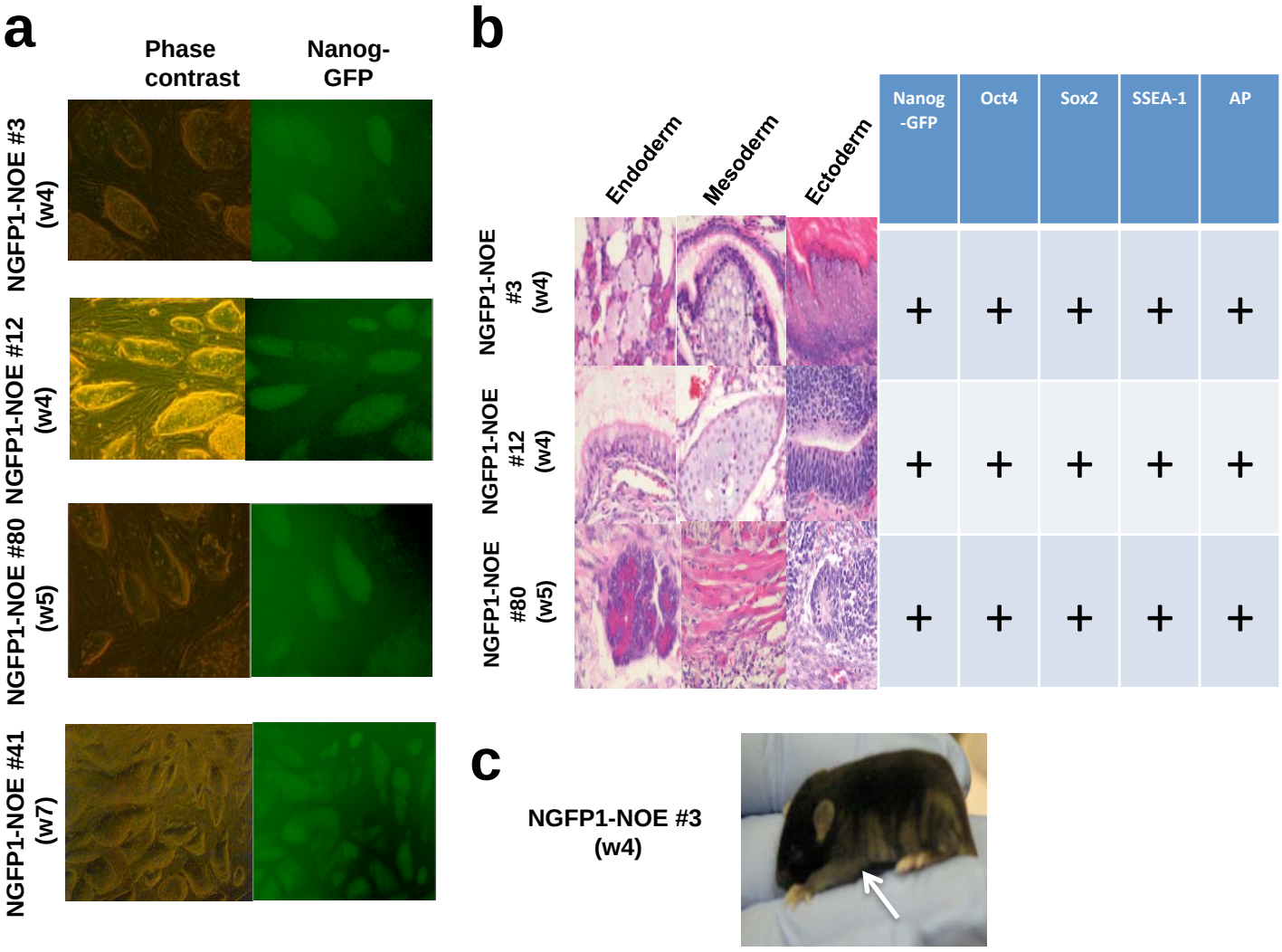

Supplementary Figure 15 | Characterization of NGFP1-NanogOE B cell derived iPSC clones. Clone # is indicated for each panel and time on DOX required to derive each line is indicated in parenthesis (w; weeks on DOX). **a,** Randomly selected NGFP1-NOE derived iPSC lines maintained ES-like morphology and remained Nanog-GFP+ independent of DOX. **b,** Well differentiated teratomas were derived from all lines tested with evident formation of endoderm, mesoderm and ectoderm structures. Table on the right summarizes the results of immuno-staining / fluorescent detection of the indicated markers on the DOX independent iPSC clones derived. Clone # is indicated for each panel and time on DOX required to derive each line is indicated in parenthesis (W; weeks on DOX). **c,** Chimera generated following injecting NGFP1-NOE #3 iPSC clone derived following 4 weeks on DOX induction *in vitro*. Chimerism is evident by the agouti coat color.

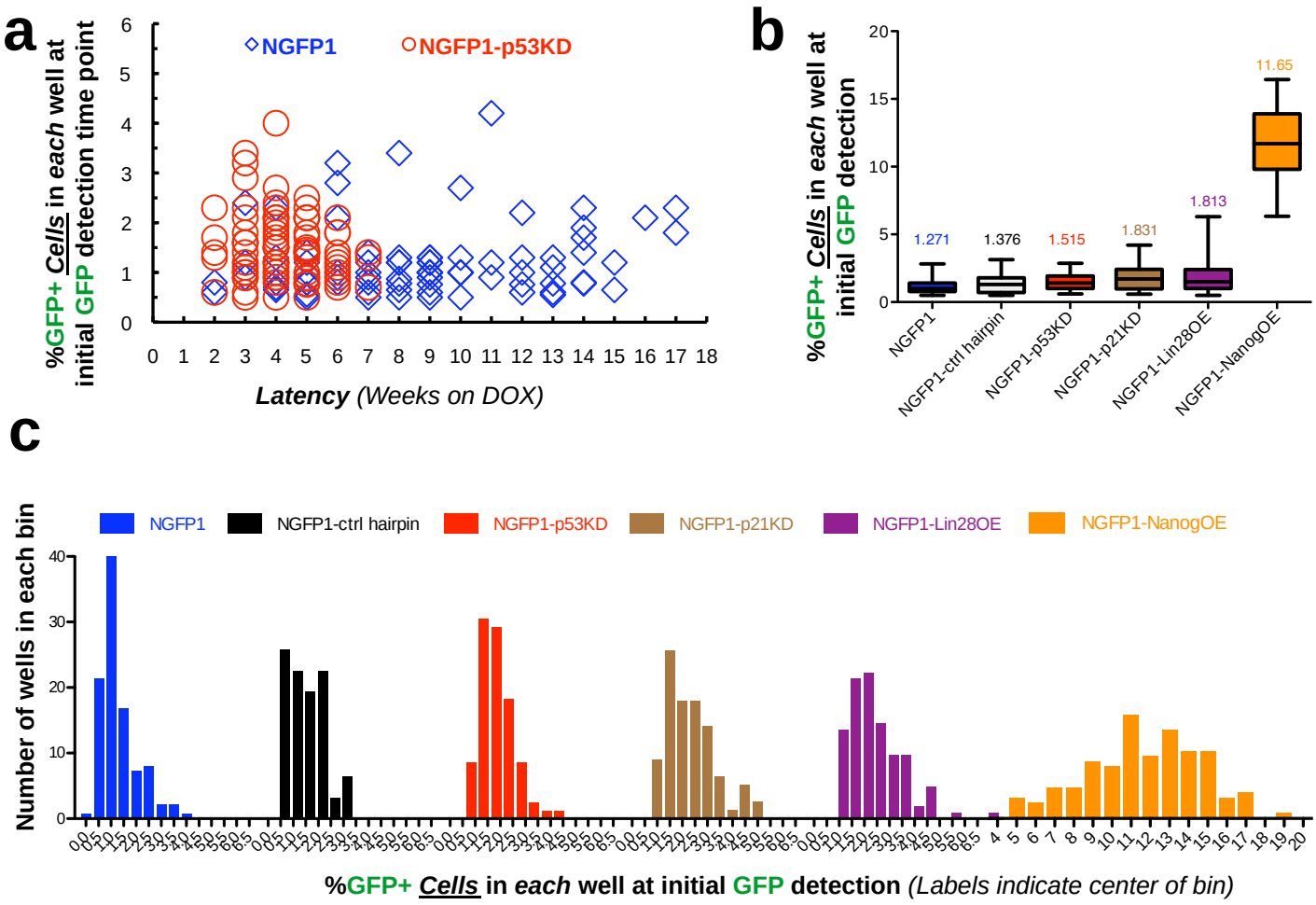

Supplementary Figure 16 | Fraction of iPSCs detected for each B cell population at first detection of GFP signal. a, Percentage of %Nanog-GFP+ cells for each individual well at the week when GFP was initially detected (>0.5% GFP+). As shown here for NGFP1 and NGFP1-p53KD wells, the %Nanog-GFP+ cells at initial time of detection in a given well of all populations was independent of the time on DOX treatment. **b,** The average value of GFP+ fraction in the populations upon initial detection of a positive signal (defined >0.5% in the study; see Supplementary Fig. 2) is shown here for all NGFP1 B cell types. The average value is listed and plotted in the center of the box. The whiskers delineate the 95% confidence interval, while the edges of the box are 25% and 75% percentiles. Comparison indicates a significant difference between NGFP1 and NGFP1-NanogOE lines ($p<0.05$), but no significant difference between NGFP1 and the other populations ($p>0.05$). We attribute this increase in the NanogOE case to the higher selection of iPSCs possibly resulting from 1) enhanced growth of Nanog overexpressing stem cells (Darr et al. *Stem Cells* 2006) and 2) a possible delay between entry into the pluripotent state by the Nanog transgene before the endogenous Nanog-alleles are reactivated (Silva et al. *Cell* 2009). **c,** A histogram of the values shown in part a, as well as for the other NGFP1 B cell types used in this study. Note the change in bins for the NGFP1-NanogOE wells.

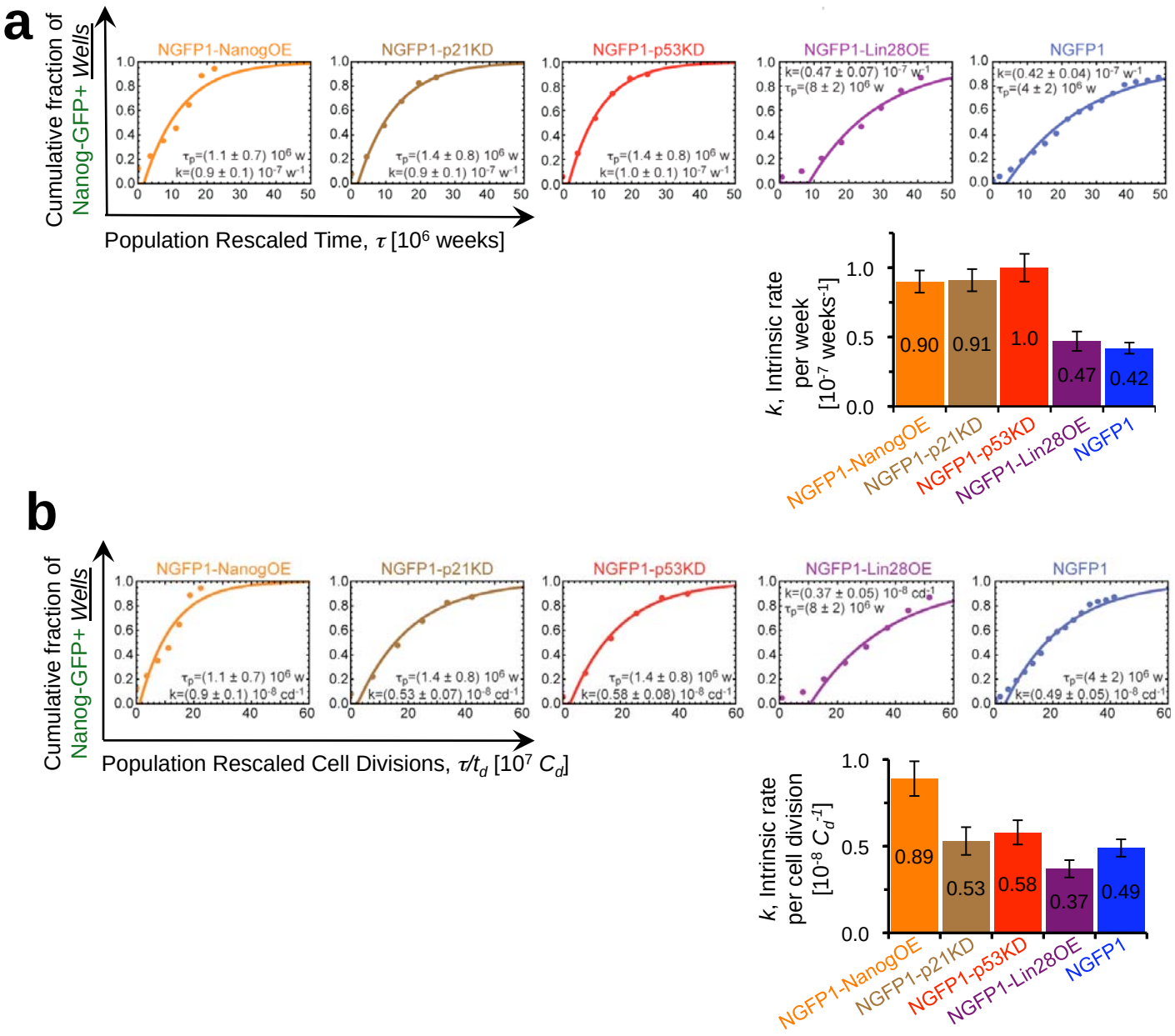

Supplementary Figure 17 | Analytical modeling results with two parameter fits. a & b, Plots of the experimental and modeling results in Fig. 4d & e respectively, but leaving the population-rescaled average proliferation time, τ_p, as an extra fit parameter (see Fig. 4a for analytical model details). Given these fitted rates, our conclusions remain unchanged, as they are based on relative changes between the rates and not absolute values. Error bars indicate 95% confidence intervals.

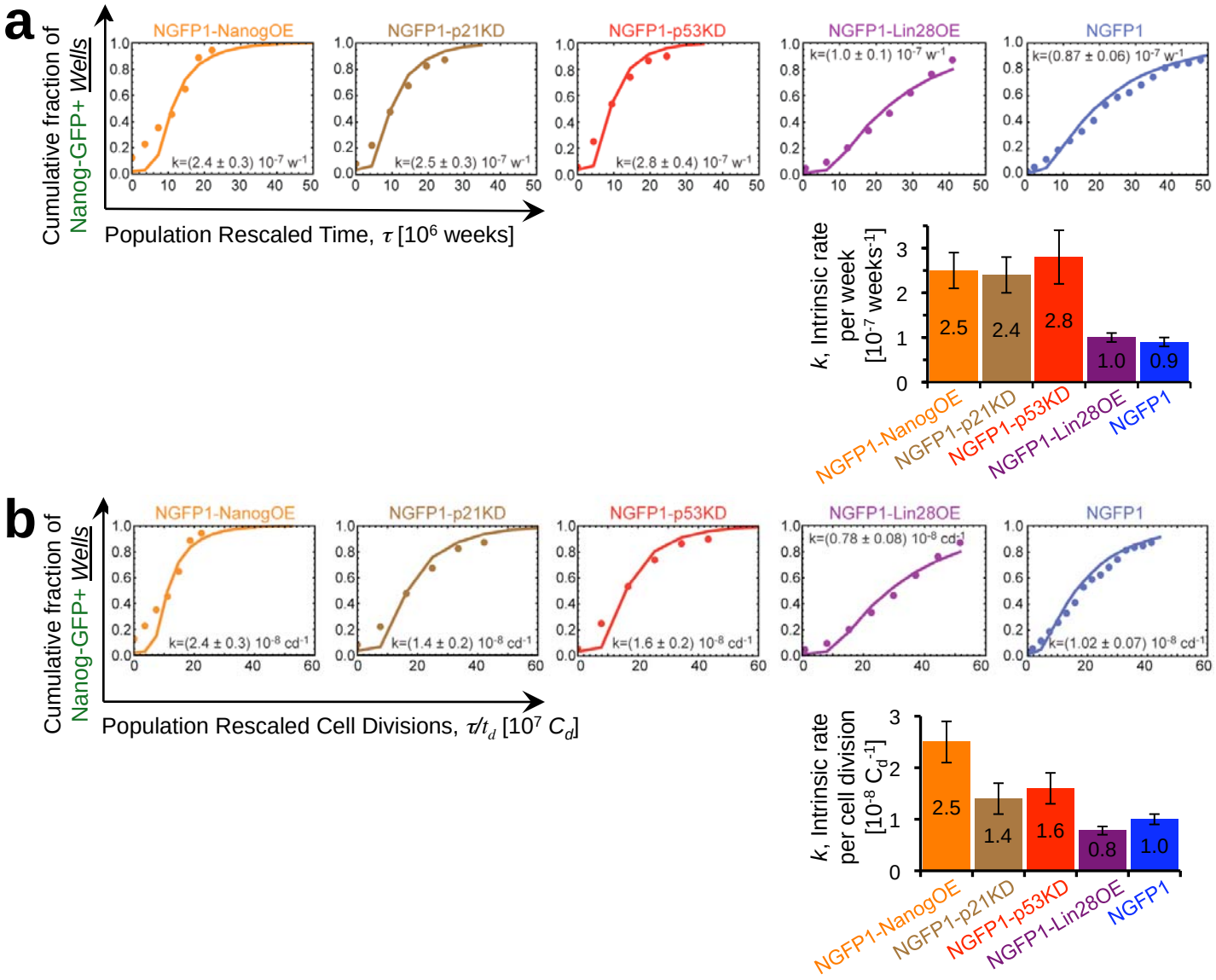

Supplementary Figure 18 | Computational simulation of reprogramming. To take into account factors like stochasticity in cell division times, fluctuations in the number of cells and potential loss of iPSCs during culturing in addition to the stochasticity in the cell-intrinsic reprogramming process, we implemented a detailed computer simulation of each experiment in this study. Comparison of the simulations and experimental data are shown in **a** in terms of population rescaled time, and in **b** in terms of population rescaled cell divisions. Given these fitted rates, our conclusions remain unchanged, as they are based on relative changes between the rates and not absolute values. Error bars indicate 95% confidence intervals.

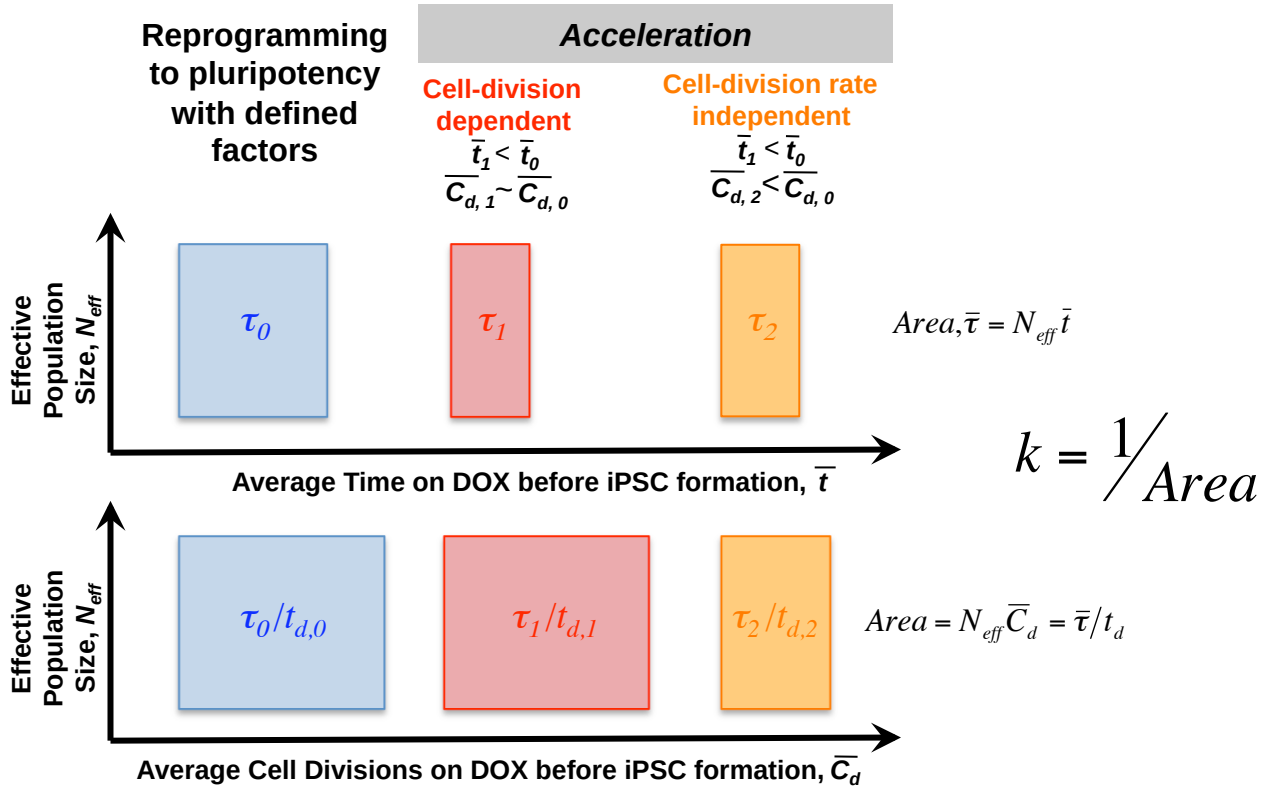

Supplementary Figure 19 | Summary of two distinct modes of accelerating reprogramming. Nearly all secondary somatic donor cells in our system can give rise to iPSCs upon continued proliferation and induction of the four reprogramming factors *in vitro*. Although the majority of clonal populations eventually produce iPSCs, the latency is not constant for each clonal population. The top x-axis represents the average latency time during factor expression, while the bottom x-axis is the average number of cell divisions during latency. The y-axes represent the effective number of cells maintained during the experiment (see Fig. 4). Under our experimental conditions, N_{eff}, remained nearly constant over the course of the experiment, and therefore population rescaled time, τ, is simply the $N_{eff}t$, the area of the square. In order to describe the population rescaled number of cell divisions during latency, the time axis is rescaled by the doubling time, t_d. The intrinsic rate of reprogramming is the inverse of the average τ. Blue scheme (left) summarizes the NGFP1 case. Red scheme (middle) represents a cell doubling time dependent scenario of accelerating the reprogramming process. As exemplified in p53/p21 pathway inhibition experiments, reprogramming kinetics are accelerated in a manner directly proportional to the augmentation of cell population doubling time, however the average number of cell divisions required to achieve full reprogramming is not influenced (still $C_{d,0}$). Orange scheme (right) represents a cell doubling time independent scenario (e.g., Nanog overexpression) of accelerating the reprogramming process where the occurrence of required unknown secondary stochastic events is enhanced and achieved within a fewer number of cell divisions on average (cell divisions << $C_{d,0}$). Notably, the different modes need not to be mutually exclusive as certain perturbations could enhance or inhibit reprogramming via both cell proliferation dependent and independent effects.